Molecular Therapy
Nucleic Acids
Original Article

Adeno-Associated Virus-Mediated RNAi against Mutant Alleles Attenuates Abnormal Calvarial Phenotypes in an Apert Syndrome Mouse Model

Fengtao Luo,[1,4] Yangli Xie,[1,4] Zuqiang Wang,[1] Junlan Huang,[1] Qiaoyan Tan,[1] Xianding Sun,[1] Fangfang Li,[1] Can Li,[1] Mi Liu,[1] Dali Zhang,[1] Meng Xu,[1] Nan Su,[1] Zhenhong Ni,[1] Wanling Jiang,[1] Jinhong Chang,[1] Hangang Chen,[1] Shuai Chen,[1] Xiaoling Xu,[2] Chuxia Deng,[2] Zhugang Wang,[3] Xiaolan Du,[1] and Lin Chen[1]

[1]Laboratory for the Rehabilitation of Traumatic Injuries, Center of Bone Metabolism and Repair, State Key Laboratory of Trauma, Burns and Combined Injury, Trauma Center, Research Institute of Surgery, Daping Hospital, Third Military Medical University, Chongqing 400042, China; [2]Faculty of Health Sciences, University of Macau, Macau SAR, China; [3]State Key Laboratory of Medical Genomics, Research Center for Experimental Medicine, Ruijin Hospital Affiliated to Shanghai Jiao Tong University School of Medicine, Shanghai 200025, China

Apert syndrome (AS), the most severe form of craniosynostosis, is caused by missense mutations including Pro253Arg(P253R) of fibroblast growth factor receptor 2 (FGFR2), which leads to enhanced FGF/FGFR2-signaling activity. Surgical correction of the deformed skull is the typical treatment for AS. Because of constant maldevelopment of sutures, the corrective surgery is often executed several times, resulting in increased patient challenge and complications. Biological therapies targeting the signaling of mutant FGFR2 allele, in combination with surgery, may bring better outcome. Here we screened and found a small interfering RNA (siRNA) specifically targeting the *Fgfr2-P253R* allele, and we revealed that it inhibited osteoblastic differentiation and matrix mineralization by reducing the signaling of ERK1/2 and P38 in cultured primary calvarial cells and calvarial explants from Apert mice ($Fgfr2^{+/P253R}$). Furthermore, AAV9 carrying short hairpin RNA (shRNA) (AAV9-*Fgfr2*-shRNA) against mutant *Fgfr2* was delivered to the skulls of AS mice. Results demonstrate that AAV9-*Fgfr2*-shRNA attenuated the premature closure of coronal suture and the decreased calvarial bone volume of AS mice. Our study provides a novel practical biological approach, which will, in combination with other therapies, including surgeries, help treat patients with AS while providing experimental clues for the biological therapies of other genetic skeletal diseases.

INTRODUCTION

Craniosynostosis, a craniofacial birth defect, is characterized by the premature fusion of one or multiple cranial sutures of skulls, with an incidence of approximately 1 in 2,500 live births.[1,2] To date, over 100 kinds of genetic syndromes have been found to have craniosynostosis.[3] Apert syndrome (AS) (OMIM: 101200), the most severe form of craniosynostosis, is characterized by synostosis of coronal sutures, midfacial hypoplasia, and syndactyly of hands and feet. Over the past two decades, our understanding of the underlying molecular mechanisms of AS has been greatly advanced. Typically, AS is caused by one of two missense mutations in adjacent amino acids of fibroblast growth factor receptor 2 (FGFR2), Ser252Trp(S252W), and Pro253Arg(P253R), which leads to overactivated FGF/FGFR2 signaling.[4,5]

To further dissect the underlying mechanisms and find novel cures for AS, we and Wang et al.[6–10] have established two mouse models independently, $Fgfr2^{+/S252W}$ and $Fgfr2^{+/P253R}$ mice, mimicking human AS using a knockin approach. These two mouse models exhibit abnormal phenotypes similar to those of Apert patients, including smaller body size, premature fusion of cranial base synchondroses and coronal suture (CS), dome-shaped skulls, midfacial hypoplasia, and syndactyly of hands or feet. We have reported that the AS mice showed rostrocaudally shortened skull dimensions and mediolaterally broadened width of the distance between the two orbits.[11] The calvarias, facial bone, cranial base, and brain are all abnormally developed in AS mice.[12–14] Nagata and colleagues[15] found that the shortening of cranial base resulting from accelerated chondrocytic differentiation was the primary reason for the acrocephalic feature in AS mice. For molecular mechanisms, several studies have revealed that the levels of phosphorylated extracellular signal-regulated kinase 1/2 (ERK1/2) and P38, the main downstream pathways of FGF/FGFR signaling, were enhanced in AS mice.[8,9,16] These findings demonstrate that these AS mouse models are good models for evaluating the therapeutic effect for AS.

Received 4 April 2018; accepted 19 September 2018;
https://doi.org/10.1016/j.omtn.2018.09.012.

[4]These authors contributed equally to this work.

Correspondence: Lin Chen, Laboratory for the Rehabilitation of Traumatic Injuries, Center of Bone Metabolism and Repair, State Key Laboratory of Trauma, Burns and Combined Injury, Trauma Center, Research Institute of Surgery, Daping Hospital, Third Military Medical University, Chongqing 400042, China.
E-mail: linchen70@163.com
Correspondence: Xiaolan Du, Laboratory for the Rehabilitation of Traumatic Injuries, Center of Bone Metabolism and Repair, State Key Laboratory of Trauma, Burns and Combined Injury, Trauma Center, Research Institute of Surgery, Daping Hospital, Third Military Medical University, Chongqing 400042, China.
E-mail: dxl_xiaolan@163.com

Surgical correction of the deformed skull is the current treatment of AS. Because of the progressive skull maldevelopment, the surgery for AS is often executed several times, resulting in increased patient challenge and complications.[17] Biological therapies targeting the FGF/FGFR signaling may bring better outcome.[18] In fact, several studies have explored the effects of biological inhibition of the molecular pathways activated in AS on skull phenotypes. Yokota et al.[19,20] found a soluble form of FGFR2 with Ser252Trp mutation can partially alleviate the phenotype of Apert mouse model by alleviating the premature closure of coronal suture in cultured calvarias and transgenic mice. PD98059, an MEK1 inhibitor, was found to reduce coronal suture fusion in cultured calvarias of $Fgfr2^{+/P253R}$ mice.[8] Inhibiting the MEK1/2 by U0126 alleviates the craniosynostosis phenotypes in $Fgfr2^{+/S252W}$ mice.[16]

The above-described molecules do not specifically antagonize the mutant FGFR2 itself, which may bring undesired effects. RNAi, in contrast, could be a powerful tool to specifically inhibit the expression of mutant alleles at the transcriptional level.[21,22] By RNAi, we could specifically silence the mutant allele to treat human diseases caused by gain-of-function mutations while leaving the expression of the wild-type (WT) allele undisturbed.[23] For AS, we previously expressed a short hairpin RNA (shRNA) specifically targeting the *Fgfr2-S252W* allele genetically in mice, and we found that the shRNA effectively alleviated the abnormal skeletal phenotypes *in vivo*.[16] However, the constitutive transgenic expression of RNAi in mice cannot be used in the clinic setting. To date, the therapeutic effect of exogenously applied RNAi on Apert phenotypes remains unknown.

Safety and efficiency are the major concerns for the application of RNAi-related therapeutics.[24] The delivery of naked small interfering RNA (siRNA) into the living body is challenging, mainly because of its rapid degradation.[25,26] Viral delivery of the interested genes has been proven to be an efficient approach for gene therapy *in vivo*.[27] Adeno-associated virus (AAV) has unique advantages over other viral vectors, i.e., low pathogenicity, reliable safety, and high efficiency.[28,29] Besides, AAV has been proven to be the effective means to deliver genes to bone tissue.[30] Here we screened and found a siRNA specifically targeting the *Fgfr2-P253R* allele, and we confirmed its effects on cultured primary calvarial osteoblasts and calvarial explants from Apert mice ($Fgfr2^{+/P253R}$). Furthermore, AAV-mediated shRNA was delivered to AS mice by local injection to evaluate its effects *in vivo* on the calvarial phenotype. Our results show that the shRNA against mutant *Fgfr2* attenuated the premature fusion of coronal suture and the decreased bone volume (BV) of parietal bone in AS mice.

RESULTS

Screening of a siRNA that Specifically Targets against the Mutant *Fgfr2* Allele

The *Fgfr2-P253R* mutant allele in mice contains a guanine (G) at position 60 of the exon 7, whereas the WT *Fgfr2* DNA bears a cytosine (C) at this position. To obtain a SNP-specific siRNA with only a single base difference that can distinguish between the mutant and WT *Fgfr2* mRNAs, we synthesized a set of siRNAs designated S1–S11. Each siRNA fully matches the *Fgfr2-P253R* mRNA but contains a C:C mismatch with WT mRNA (Figure 1A). The 11 siRNAs were individually transfected into primary osteoblasts from Apert mice for assessing their silencing effects on the expressions of mutant *Fgfr2*. Real-time PCR revealed that the expression levels of both the total *Fgfr2* and mutant *Fgfr2* were reduced in S2-, S4-, S7-, S8-, S9-, S10-, and S11-treated osteoblasts. Among them, S2 showed the most remarkable silencing effect on the expression of mutant *Fgfr2*. There were no significant changes in the expression levels of mutant *Fgfr2* in S1-, S3-, S5-, and S6-treated osteoblasts (Figures 1B–1D; the results from S4 to S11 are not shown).

Western blotting was employed to further evaluate the effects of S1–S11 on FGFR2 expression. Western blots revealed that S4, S7, S8, S9, S10, and S11 reduced the expression of FGFR2, whereas S1, S2, S3, S5, and S6 did not downregulate the FGFR2 level in WT osteoblasts (Figure 1E). Treatment of S2, S4, S7, S10, and S11 led to decreased protein levels of FGFR2 in the primary osteoblasts derived from Apert mice, which contain WT and mutant *Fgfr2* alleles. S2 exhibited the strongest inhibitory effect on FGFR2 protein level (Figures 1E and 1F; the results from S4 to S11 are not shown). Thus, S2 was employed as the mutant *Fgfr2*-specific siRNA for the subsequent experiments.

S2 Treatment Decreases the Osteogenic Differentiation and Matrix Mineralization of Apert Osteoblasts by Downregulating ERK1/2 and P38 MAPK Pathways

To assess the effects of S2 on the proliferation and differentiation of osteoblasts, primary calvarial osteoblasts from Apert mice and their littermates were used to detect the changes of these parameters and related signaling pathways following S2 treatment. The expression level of FGFR2 was significantly decreased in S2-treated Apert osteoblasts compared with scramble siRNA- (negative control- [NC-]) treated Apert osteoblasts. In addition, when compared with S2-treated WT osteoblasts, the expression of total FGFR2 was significantly decreased in S2-treated Apert osteoblasts, but there was no significant difference in the FGFR2 expression between the NC- and the S2-treated WT group, indicating that S2 discriminably knocked down the expression of *Fgfr2-P253R* (Figures 2A and 2B).

It has been found that *Fgfr2-P253R* leads to the accelerated differentiation of osteoblasts through the mitogen-activated protein kinase (MAPK) pathways, including ERK1/2 and P38, which play important roles in calvarial development.[8,9] We then detected the levels of phosphorylated ERK1/2 and P38 in WT and Apert osteoblasts treated with S2 or NC. In the absence of S2 treatment, Apert osteoblasts had higher phosphorylated levels of ERK1/2 and P38 than did WT osteoblasts (Figures 2A, 2C, and 2D). Although the level of phosphorylated P38 in S2-treated Apert osteoblasts was higher than that in S2-treated WT osteoblasts, S2 treatment significantly decreased the phosphorylation levels of ERK1/2 and P38 of Apert osteoblasts

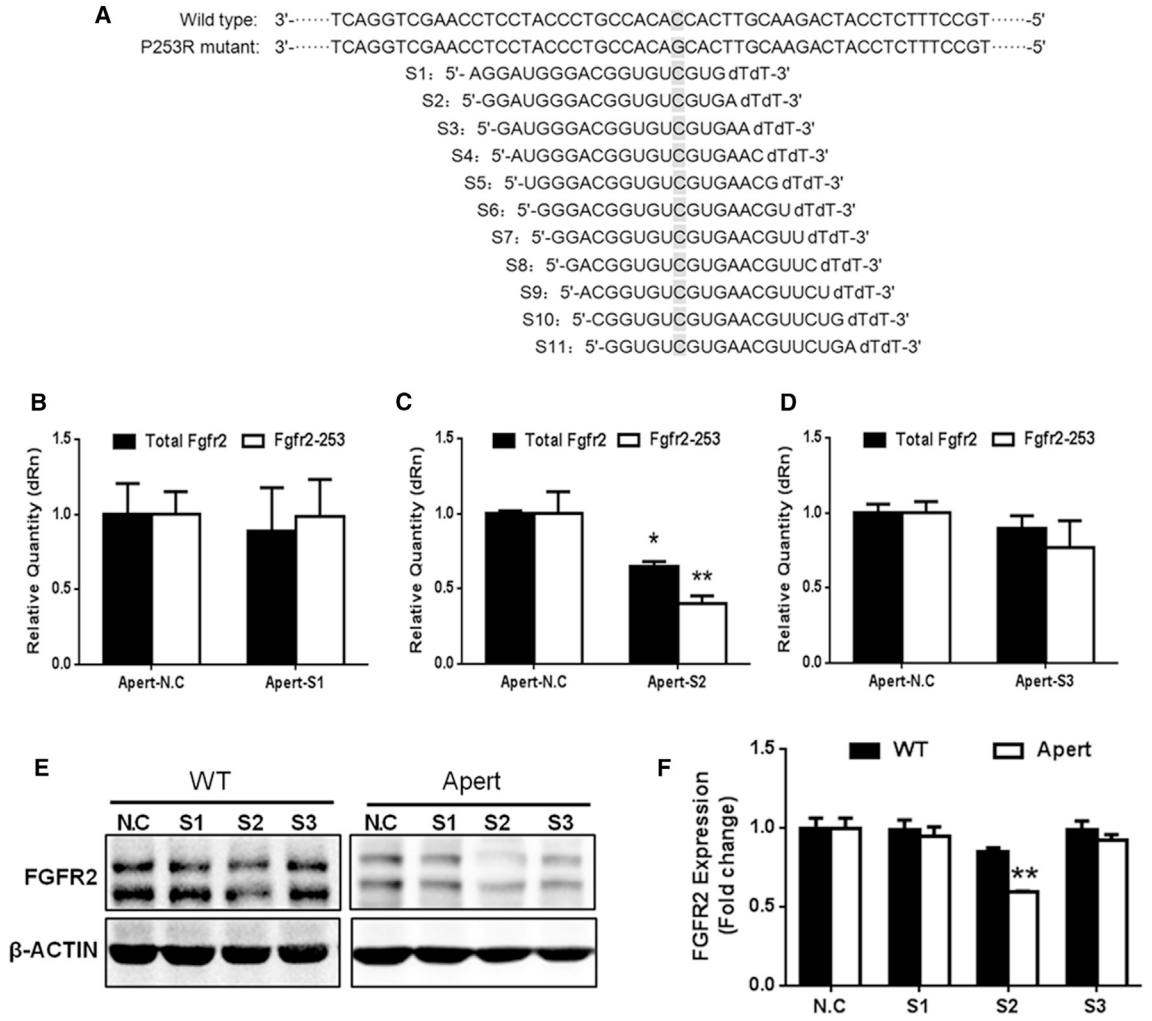

Figure 1. Screening of siRNA that Specifically Silences the Fgfr2-P253R Mutant Allele in Apert Osteoblasts

Serial siRNAs (S1–S11) were designed to target mutant allele. (A) Each siRNA fully matches the Fgfr2-P253R mRNA but contains a C:C mismatch with wild-type mRNA. (B–D) The effect of S1 (B), S2 (C), and S3 (D) on the expressions of total Fgfr2 and mutant Fgfr2. (E) Western blotting revealed that S2 significantly decreased FGFR2 expression in Apert osteoblasts. (F) Quantified measurement of the western blot (WB) bands showed that S2 significantly decreased the expression of FGFR2. Data are presented as mean ± SD. WT, calvarial osteoblasts of wild-type mice; Apert, calvarial osteoblasts of Apert mice. (*$p < 0.05$ and **$p < 0.01$; $n = 3$ in each group).

compared with NC-treated Apert osteoblasts, indicating that S2 alleviated the activation of ERK1/2 and P38 signaling caused by the FGFR2-P253R mutation (Figures 2A, 2C, and 2D). Together, these results demonstrate that S2 treatment decreased the expression of mutant FGFR2 and, subsequently, reduced the levels of phosphorylated ERK1/2 and P38.

The proliferation of osteoblasts from Apert mice showed no significant change compared with that of WT osteoblasts (data not shown). In Apert osteoblasts, alkaline phosphatase (ALP) staining revealed that S2 treatment led to a decreased number of osteoblasts with crystal violet staining compared with that in the NC siRNA-treated group (Figure 2E). Alizarin red staining revealed that the mineralization was significantly accelerated in the Apert osteoblasts compared with that of WT osteoblasts. Following S2 treatment, WT osteoblasts showed no significant changes in mineralization compared with NC siRNA-treated osteoblasts, whereas the accelerated mineralization in the Apert osteoblasts was significantly reduced (Figure 2F), indicating that S2 treatment effectively alleviated the increased mineralization of Apert osteoblasts. The mRNA levels of several osteoblastic differentiation-related genes were detected by using real-time qPCR. We found that, compared with those of WT osteoblasts, the expression levels of *Runx2*, *Collagen 1*, *Osteocalcin*, and *Osteopontin* were increased in Apert osteoblasts in the absence of S2 treatment, and these were significantly reduced by S2 treatment. When compared with the S2-treated WT group, the expression levels of *Runx2* and *Collagen 1* were significantly decreased in the S2-treated Apert osteoblasts (Figures 2G–2J).

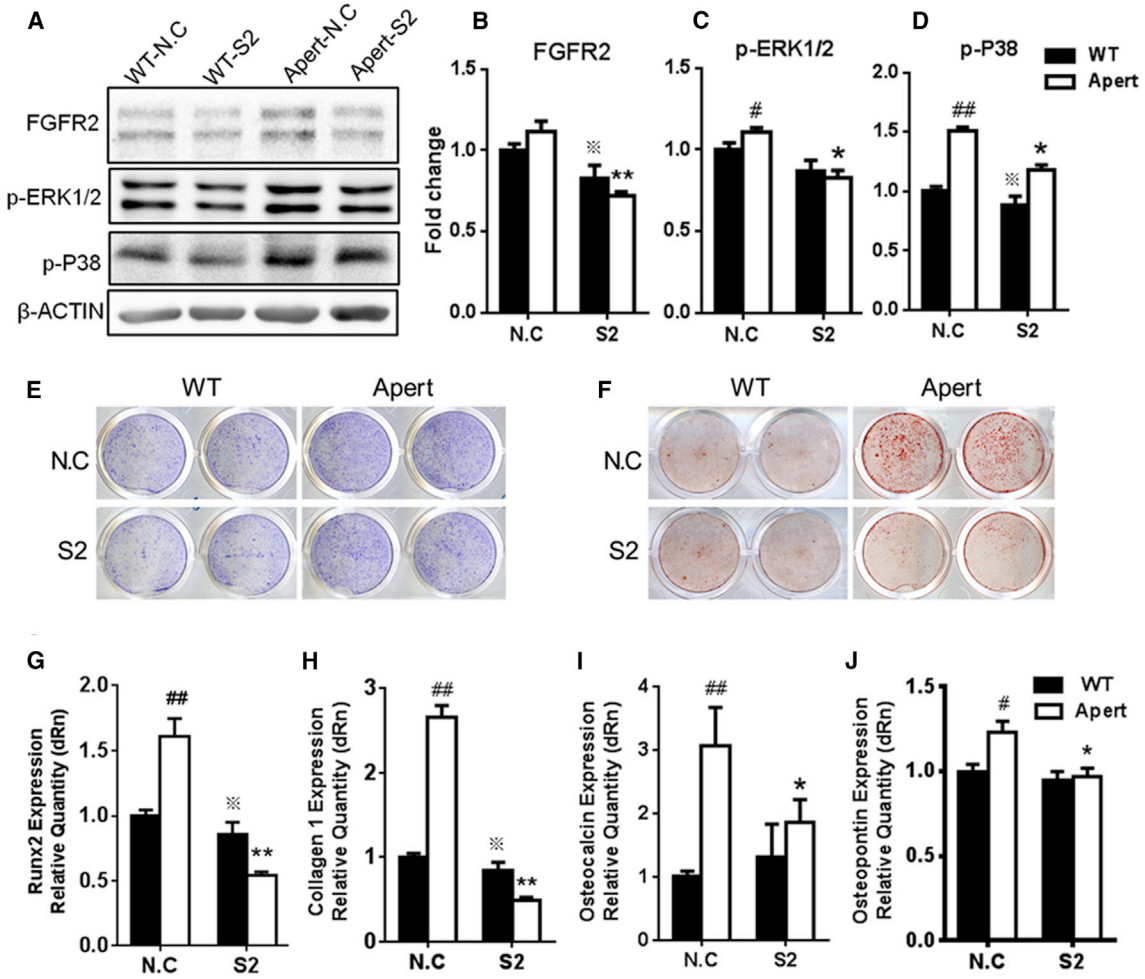

Figure 2. S2 Treatment Attenuated the Differentiation and Matrix Mineralization of Apert Osteoblasts by Downregulating ERK1/2 and P38 Pathways

(A) The protein levels of FGFR2, the phosphorylated ERK1/2, and P38 were downregulated by S2 treatment. Densitometric analysis of the bands indicated that S2 treatment downregulated the protein levels of FGFR2 (B), the phosphorylated ERK1/2 (C), and P38 (D). (E) ALP staining showed that S2 treatment attenuated the differentiation of Apert osteoblasts. (F) Alizarin red staining showed matrix mineralization was increased in Apert osteoblasts, which was decreased by S2 treatment. (G–J) Real-time PCR showed that S2 treatment decreased the expressions of *Runx2* (G), *Collagen* 1 (H), *Osteocalcin* (I), and *Osteopontin* (J), indicating that S2 treatment attenuated the osteoblastic differentiation. Data are presented as mean ± SD ($^{\#}$significant change compared with NC-treated WT osteoblasts, *significant change compared with NC-treated Apert osteoblasts, $^{※}$significant change when S2-treated Apert osteoblasts were compared with S2-treated WT osteoblasts; *$p < 0.05$, **$p < 0.01$. $^{\#}p < 0.05$, $^{\#\#}p < 0.01$, and $^{※}p < 0.05$; Western blotting and real-time PCR essay, n = 3 in each group).

S2 Treatment Attenuates the Premature Closure of Coronal Sutures of the Cultured Calvarias of Apert Mice

The therapeutic effects of S2 were further evaluated in cultured calvarias. Calvarias of 5-day-old Apert and WT mice were dissected and cut into equivalent left and right parts along the midline. The left and right parts of calvarias were treated with NC or S2, respectively. After being cultured for 7 days, the premature closure of coronal sutures in Apert calvarias was accelerated compared with that of WT calvarias, while it was delayed by S2 treatment (Figure 3A). Analysis of suture fusion patterns indicated that S2-treated WT calvarias displayed similar suture fusion patterns with those of NC-treated WT calvarias. H&E staining revealed that Apert calvarias had an increased overlapping region of the osteogenic fronts of coronal sutures, which was decreased by S2 treatment (Figure 3B).

In addition, results from three-dimensionally reconstructed micro-computed tomography (micro-CT) images showed that the thickness of parietal bone was significantly decreased in Apert calvarias compared with that of WT calvarias. The thickness of parietal bone in Apert mice was 31.94% thinner than that of WT calvarias (Figure 3D). With the treatment of S2, the decreased thickness of parietal bone was rescued in Apert calvarias (Figure 3C). S2-treated Apert calvarias had a 24.78% increase in the thickness of parietal bone (Figure 3D). Further analysis revealed that S2 efficiently attenuated the decrease of parietal BV (Figure 3E). The bone mineral density

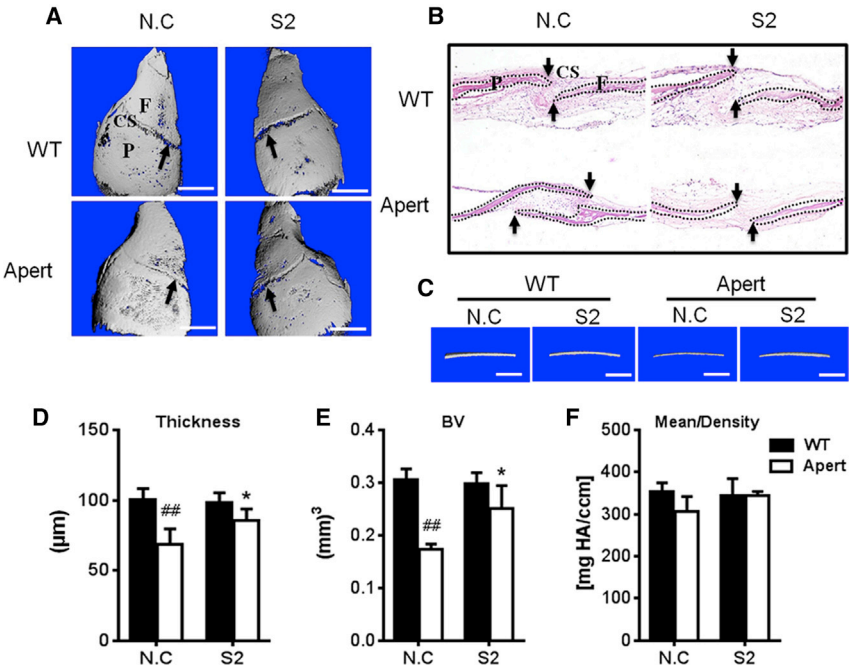

Figure 3. S2 Treatment Attenuated the Premature Closure of Coronal Sutures of Cultured Calvarias

(A) Micro-CT images of the calvarias revealed that coronal suture was closed in Apert calvarias, whereas S2 treatment attenuated the premature closure. (B) Apert calvarias showed an increased overlapping region between parietal bone and frontal bone, as revealed by H&E staining of sections, while S2 treatment decreased the overlapping of osteogenic fronts. (C) 3D-constructed images revealed that S2 treatment increased the thickness of Apert calvarial bone. (D) The thickness of parietal bone was decreased in Apert mice compared with WT calvarias. With S2 treatment, the thickness of parietal bone was increased compared with NC-treated Apert calvarias. (E) Micro-CT analysis of the parietal bone revealed that S2 treatment attenuated the decreased bone volume (BV) of Apert calvarias. (F) The BMD showed no significant difference between NC- and S2-treated Apert calvarias. P, parietal bone; F, frontal bone; CS, coronal suture. Black arrows indicate osteogenic fronts. Data are presented as mean ± SD (*significant change compared with NC-treated Apert calvarias, $^{\#}$significant change compared with NC-treated WT calvarias; $^{*}p < 0.05$ and $^{\#\#}p < 0.01$; WT-NC, n = 6; WT-shRNA, n = 5; Apert-NC, n = 7; Apert-shRNA, n = 6). White scale bar, 1 mm.

(BMD) of Apert calvarias had no significant change between NC- and S2-treated groups (Figure 3F). These data demonstrate that S2 treatment partially rescued the maldevelopment of Apert calvarias.

Screening for AAV Serotypes with High Infection to Calvarias

The viral delivery of genes was proven to be an efficient approach for gene therapy *in vivo*.[27] AAVs have important advantages over other viral vectors, i.e., low pathogenicity, high safety, and long-term transgene expression. To date, a few studies have explored the efficiency of AAV-based gene delivery to bone tissue.[30,31] Considering that different serotypes of AAV have variable affinities to bone, we analyzed the infecting effect on mouse calvarias of AAV2, AAV5, AAV9, and AAV-DJ serotypes. The PBS (control), AAV2-GFP, AAV5-GFP, AAV9-GFP, and AAV-DJ-GFP were subcutaneously injected into the calvarias of mice at post-natal day 0. The calvarias of mice were harvested to detect the expression of GFP reporter at 5 days after injection.

All four of the AAV serotypes could infect cells of calvarias with variable efficacies, as evidenced by GFP fluorescence intensities. Among them, AAV2-GFP and AAV9-GFP exhibited stronger GFP signals in parietal bone, frontal bone, and sutures, whereas AAV5-GFP- and AAV-DJ-GFP-infected calvarias had milder fluorescence intensity than those infected by AAV2-GFP and AAV9-GFP (Figures 4A–4E). Then, we investigated the GFP expression of calvarias 30 days after injection with PBS (control), AAV2-GFP, and AAV9-GFP. Our results revealed that AAV9-GFP-injected calvarias had stronger GFP expression than that of AAV2-GFP-injected calvarias (Figures 4F and 4G), suggesting that the AAV9 viral serotype is suitable for delivering genes to be expressed for a long term in calvarias (Figure 4H). Thus, we employed the AAV9 viral serotype to deliver RNAi for *in vivo* treatment of Apert mice.

AAV9-Mediated shRNA Treatment Attenuates the Premature Closure of Coronal Suture and the Decreased BV of Apert Mice *In Vivo*

To evaluate the *in vivo* therapeutic effects of shRNA on the calvarial phenotypes of Apert mice, AAV9-*Fgfr2*-shRNA viruses were locally injected twice on calvarias of Apert mice at day 0 and day 4. Then 6 days later, calvarias of shRNA-treated Apert and WT mice were dissected to evaluate the gene expressions. The expression of total *Fgfr2* (including WT and mutant alleles) was not significantly varied between NC- and shRNA-injected WT mice. However, there was a significant decrease of total *Fgfr2* expression level in Apert calvarias after shRNA treatment compared with that of the NC-treated Apert mice (Figure 5A). *Fgfr2* expression was significantly decreased in shRNA-treated Apert mice compared with shRNA-treated WT mice, indicating that shRNA preferably knocked down the expression of mutant *Fgfr2* in mice (Figure 5A). Expectedly, our results showed that the expression of the *Fgfr2-P253R* allele was not detected in WT mice (data not shown). After shRNA injection, the expression of mutant *Fgfr2* was dramatically reduced in Apert calvarias, indicating that AAV-mediated shRNA worked efficiently in calvarias (Figure 5B). Besides, the expressions of *Collagen 1* and *Runx 2* were significantly increased in Apert mice compared with those of WT mice, which were decreased after shRNA injection (Figures 5C and 5D).

Three-dimensional reconstruction of micro-CT images revealed that shRNA injection significantly attenuated the premature closure of coronal suture in day 20 Apert mice (Figure 5E), while

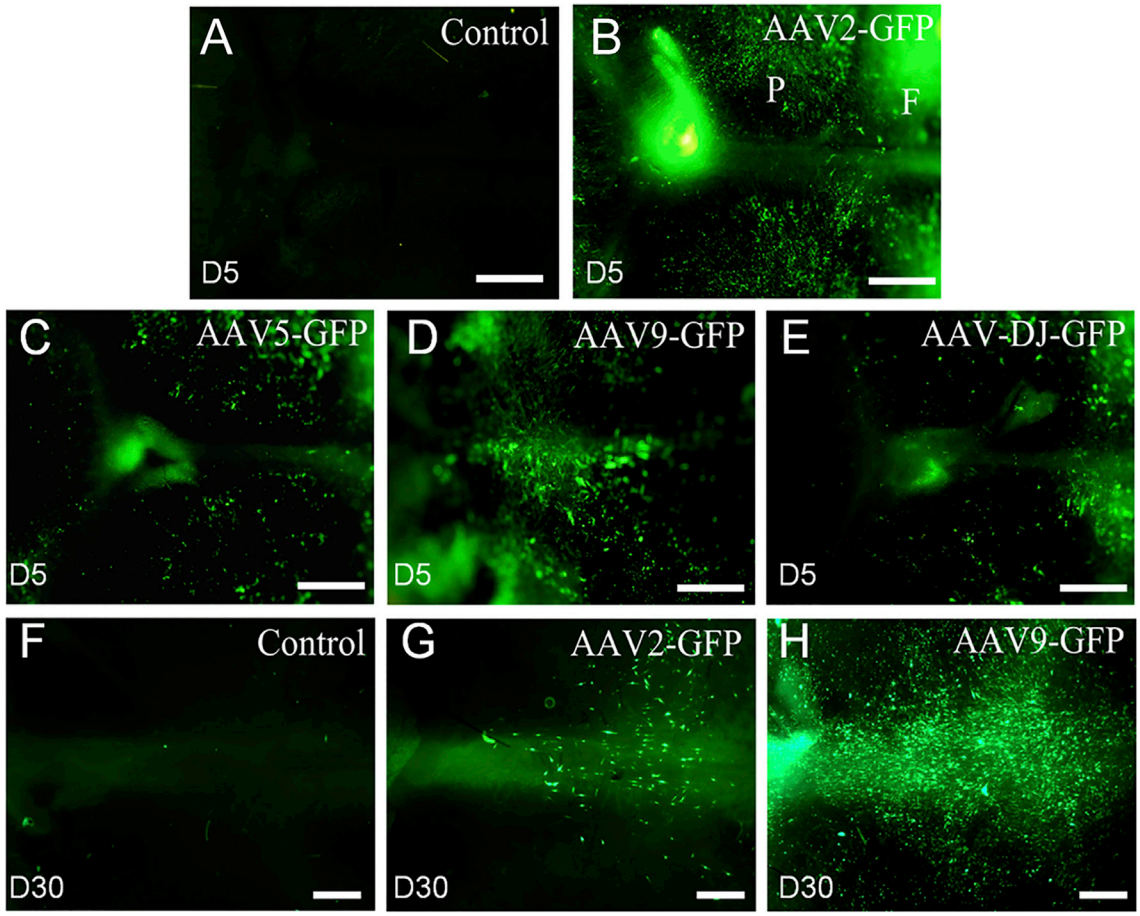

Figure 4. AAV9 Effectively Mediated Reporter Gene Expression in Calvarial Bone

(A–E) Detection of GFP fluorescence of calvarias at 5 days after injection of PBS (A), AAV2-GFP (B), AAV5-GFP (C), AAV9-GFP (D), and AAV-DJ-GFP (E), respectively. (F–H) GFP fluorescence was detected at 30 days after the injection of PBS (F), AAV2-GFP (G), and AAV9-GFP (H). P, parietal bone; F, frontal bone (n = 3 in each group at per time point). White scale bar, 2 mm.

shRNA- and NC-treated WT mice displayed similar suture fusion patterns. About 53.85% of the Apert calvarias displayed fused coronal suture, while about 10.00% of coronal sutures were fused in WT calvarias. The shRNA treatment partially rescued the premature closure of coronal sutures of Apert calvarias compared with that of NC treatment (Figure 5F). Histological analysis revealed that shRNA treatment attenuated the overlapping area of osteogenic fronts in the coronal sutures of Apert skulls (Figure 5G). Without shRNA treatment, Apert mice showed reduced BV of parietal bone when compared with that of WT mice, which was partially rescued by AAV-*Fgfr2*-shRNA treatment (Figure 5H). Further micro-CT analysis indicated that shRNA efficiently attenuated the decreased BV of parietal bone (Figure 5I), while shRNA had no significant effect on the BMD of Apert calvarias (Figure 5J).

We further analyzed the calvarial morphology by using quantitative Euclidean distance matrix analysis (EDMA). Nine landmarks were defined on calvarias, and three-dimensional coordinates of post-natal day 20 WT and Apert mice were collected for EDMA (Table 1; Figure 6A). Along the rostrocaudal axis, the linear distances of calvarias, such as landmarks 1 to 2, 2 to 3, and 3 to 4, in NC- or AAV9-*Fgfr2*-shRNA-treated Apert mice, were significantly decreased when compared with NC- or AAV9-*Fgfr2*-shRNA-treated WT mice (Table 2; Figures 6B and 6C). The shRNA-treated Apert mice exhibited the trend of alleviation in the deformation of calvarial bone when compared with the NC-treated Apert mice, such as landmarks 1 to 3, 2 to 3, and 3 to 4, although these changes were not statistically significant (Table 2; Figures 6D and 6E).

DISCUSSION

Presently, the major therapy for Apert is surgery. However, AS patients have to undergo a series of surgeries throughout their lifetime and probably get serious complications.[32,33] As a genetic disease, AS is caused by gain-of-function mutations of FGFR2; we thus may use a biological approach to alleviate the severity of AS. Mutations of AS result in dysregulated downstream signaling, such as enhanced

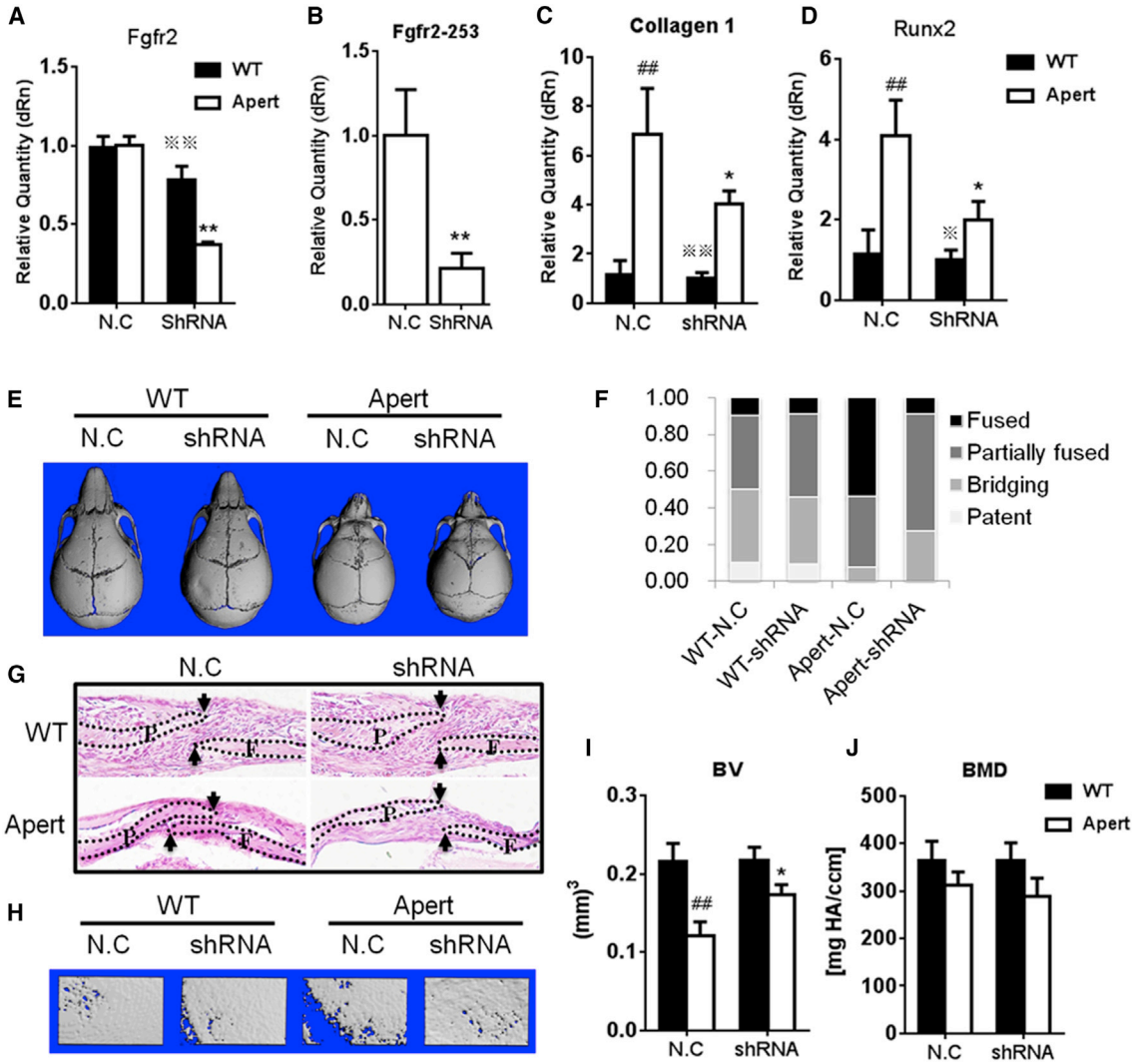

Figure 5. AAV9-Mediated shRNA Treatment Attenuated the Increased Overlapping Region of Osteogenic Fronts and the Reduced Bone Volume of Parietal Bone in Apert Mice

(A) Real-time qPCR revealed that total *Fgfr2* expression was decreased after AAV9-*Fgfr2*-shRNA treatment. (B) AAV9-*Fgfr2*-shRNA *in vivo* injection to calvarias effectively decreased the expression of *Fgfr2-P253R*. (C and D) The shRNA treatment also reduced mRNA expression of *Collagen* 1 (C) and *Runx2* (D). (E) Micro-CT images revealed that the calvarias were deformed in day 20 Apert mice, which was attenuated by shRNA treatment. (F) Suture fusion patterns in four groups of mice. Four degrees of fusion were defined: patent, white; bridging, light gray; partially fused, dark gray; and fused, black. (G) Sections with H&E staining showed an increased overlapping region between parietal bone and frontal bone in Apert calvarias, which was attenuated by shRNA treatment. (H) 3D-reconstructed images revealed that shRNA treatment attenuated the bone volume (BV) of Apert calvarial bone. (I) Micro-CT analysis of the parietal bone revealed that S2 treatment attenuated the decreased bone volume of Apert calvarias. (J) The BMD showed no significant change between NC- and shRNA-treated Apert calvarias. Data are presented as mean ± SD. P, parietal bone; F, frontal bone. Black arrows indicate osteogenic fronts (*significant change compared with NC-treated Apert mice, $^{\#}$significant change compared with NC-treated WT mice, $^{※}$significant change when S2-treated Apert mice were compared with S2-treated WT mice; $^{*}p < 0.05$, $^{**}p < 0.01$, $^{\#}p < 0.05$, $^{\#\#}p < 0.01$, $^{※}p < 0.05$, and $^{※※}p < 0.01$; WT-NC, n = 10; WT-shRNA, n = 11; Apert-NC, n = 13; Apert-shRNA, n = 11).

ERK1/2, P38, PI-3K, and PLCγ pathways, etc.[34] Theoretically, we can modulate the activities of mutant FGFR2 at multiple levels, such as inhibition of FGFs binding to FGFR2 and its downstream signaling and modulating other skeleton development-related-signaling pathways affected by mutant FGFR2, including BMP, Wnt, etc. Although the application of inhibitors against individual downstream signaling, for example, inhibition of ERK1/2, was found to attenuate the maldeveloped skull phenotypes of AS,[16] the involvement of other downstream signaling pathways, such as PI-3K/AKT, in the pathogenesis of Apert make the treatment against just one downstream pathway not the best strategy for obtaining optimal effects. Moreover, the downstream signals, such as MAPK, also participate in various events

Table 1. The Definition of Calvarial Landmarks Used in EDMA

Landmarks	Definition
1	nasion
2	bregma
3	intersection of parietal and interparietal bones
4 and 7	frontal-squasmosal intersection at temporal crest (bilateral)
5 and 8	joining of squasmosal body to zygomatic process of squasmosal (bilateral)
6 and 9	intersection of parietal, temporal, and occipital bones (bilateral)

in cells other than suture cells; inhibiting these signal pathways may bring potential risk.

In addition, the inhibitors of these downstream pathways usually have severe side effects. Given the complex cross-binding among 22 FGFs and 4 FGFRs, reducing the expressions of FGFs and the binding between FGFs and FGFR2 also have some potential side effects caused by the unwanted inhibition of multiple FGFs/FGFRs. As to the inhibition of FGFR2 itself, we can block the activity of FGFR2 at three levels: DNA, RNA, and protein. At the genomic level, recently developed CRISPR/Cas9 gene-editing techniques exhibit great potential for the gene therapy of genetic diseases, including AS. The off-target effects of CRISPR/Cas9, however, may cause permanent changes in other genes, thus limiting its clinical application. Morita et al.[19] employed a soluble form of FGFR2 with S252W mutation to partially relieve the craniosynostosis of cultured Apert calvarias. However, this approach does not specifically target FGFR2; it also inhibits other FGFRs such as FGFR1 and 3, which are important regulators of suture development. Indeed, there are no specific antagonists for either WT or mutant FGFR2 protein so far. Transcriptional regulations, without disrupting DNA sequence, such as RNAi and CRISPR interference (CRISPRi),[35] exhibit promising prospects for the treatment of AS. Furthermore, an RNAi approach can just target the mutant allele, which is an excellent approach for dominant genetic disorders resulting from gain-of-function mutations, including AS that contains a disease-causing allele and a normal WT copy. We are expected to biologically modulate the mutant allele while leaving the normal mRNA unaffected. Importantly, siRNA or shRNA targeting the mutant allele specifically is a readily available approach.

We previously found that transgenic expression of an shRNA targeting FGFR2 can effectively alleviate the abnormal skeletal phenotypes in AS mice. However, this transgenic approach used in mice cannot be used in a clinical setting. Local or systemic application of exogenous RNAi is more practical. Indeed, RNAi-based therapy (Patisiran) for transthyretin amyloidosis (ATTR) has recently been approved by the FDA for a phase 3 clinical trial.[36] We thus utilized the exogenous RNAi approach to treat AS.

To find a siRNA sequence specifically targeting the mutant *Fgfr2* allele, we compared the knocking-down effects on mutant *Fgfr2* among 11 successive siRNAs, in which the mismatch (C:C) against the WT *Fgfr2* allele is located at position 16 to 6 away from the 5′ end of the siRNA. The 5′ seed region of the siRNA is responsible for the recognition and binding to targeting mRNA; the mismatches located in this region will generally provide only moderate single-nucleotide discrimination. In contrast, mismatches in the region from the 3′ end to the seed sequence provided excellent single-nucleotide discrimination.[37,38] In accordance with this theory, our results revealed that S2 (the mismatch was located in the region from the 3′ end to the seed sequence) had the optimal discrimination between WT and mutant *Fgfr2* allele.

As valuable vehicles for gene delivery, AAVs are widely used in human and animal models, for their biological safety, low pathogenicity, long-term gene expression, and the ability to infect both dividing and quiescent cells. Numerous AAV serotypes have been identified with variable tissue-specific infectivity. There are very few reports in the literature about AAV-mediated gene therapies in bone tissue. The most commonly used AAV for bone tissue is the AAV2 serotype, which has an extensive infectivity in the majority of tissues.[30,31,39–41] Apart from AAV2, other serotypes have not been tested in bone tissue. Here, four AAV serotypes, AAV2, AAV5, AAV9, and AAV-DJ, were tested in the calvarial bone of mice. Our results showed that the AAV5 and AAV-DJ serotypes had lower infectivity compared with the AAV2 and AAV9 serotypes at an early stage after virus injection, while AAV9 drove stronger GFP expression in calvarias than did AAV2. Furthermore, AAV9-mediated GFP expression lasted longer, as evidenced by the strongest GFP expression at day 30 after local injection. We thus demonstrate that AAV9 exhibits high infectivity in the developmental calvarial bone, suggesting that it can be used for the gene therapy of a maldeveloping skeleton. Interestingly, GFP fluorescence signals were gradually reduced with the development of calvarial bone, indicating that it is necessary to have multiple injections of AAV to obtain sustained gene expression during the development of calvarial bone.

In this study, we tested the therapeutic effects of AAV-mediated shRNA on the calvarial phenotypes of AS mice. Our data showed that AAV9-mediated shRNA targeting FGFR2-P253R can specifically reduce the expression of mutant FGFR2 (FGFR2-P253R), with reduced phosphorylation levels of ERK1/2 and P38, and subsequently alleviate the phenotypes of Apert calvarias by delaying the premature fusion of coronal sutures.

Since the skull phenotypes of Apert mice were just partially rescued in this study, further studies are needed to obtain a better therapeutic outcome by finding the optimal concentrations and dosage of the AAV-RNAi and optimal timing and times of injection, etc. Specifically, targeted delivering of siRNA to suture mesenchyme or osteoblasts using respective targeting peptides or aptamers may further promote the therapeutic effect of siRNA on craniosynostosis. Considering the broad effects of mutant FGFR2, systemic application of AAV-shRNA that targets mutant Fgfr2 in more tissues, such as brain and synchondrosis, may further improve outcome. Since FGFR2 is an oncogene and FGFR2-P253R has been found in gastric cancer, our

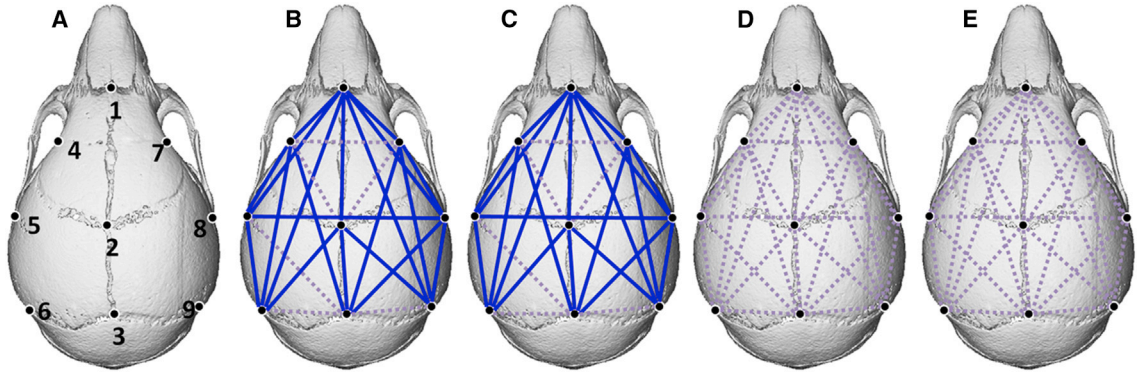

Figure 6. Schematic Diagram for EDMA of Calvarial Morphologies of Apert and WT Mice with NC or shRNA Treatment

(A) Diagram of 9 landmarks on the mouse skull. (B) Difference of calvarial morphologies between Apert and WT mice with NC treatment. (C) Difference of calvarial morphologies between Apert and WT mice with shRNA treatment. (D) Calvarial morphologies of shRNA-treated WT mice compared to NC-treated WT mice. (E) Difference of calvarial morphologies between shRNA Apert mice and NC-treated Apert mice. Blue lines show those linear distances that have a decrease of over 5%. Broken gray lines show linear distances with no significant change. NC-treated WT mice, n = 10; shRNA-treated WT mice, n = 11; NC-treated Apert mice, n = 13; shRNA-treated Apert mice, n = 11.

study also suggests that AAV-mediated *Fgfr2* RNAi may serve as a therapeutic strategy for those FGFR2 mutations related to cancer.

In summary, in this study we find an RNAi sequence specifically targeting *Fgfr2-P253R*-causing AS. We demonstrate that AAV9 is a good tool for the gene therapies for bone-related diseases, and AAV9-mediated shRNA against *Fgfr2-P253R* can partially alleviate the skull maldevelopment of the Apert mouse model. So far there are few studies testing the effects of biotherapy on craniosynostosis using *in vivo* mouse models. Our study demonstrates that exogenous RNAi is a novel practical biological approach that will, in combination with other therapies, including surgery, help not only the treatment of patients with AS but also other skeletal diseases or regeneration.

MATERIALS AND METHODS

Animals

$Fgfr2^{+/P253R\text{-}neo}$ mice have been previously described.[8] CMV-Cre mice were purchased from Jackson Laboratory. All mice were maintained on a C57BL/6J background. Apert mice ($Fgfr2^{+/P253R}$) were generated by crossing male offspring of CMV-Cre and female offspring of $Fgfr2^{+/P253R\text{-}neo}$ mice. Mice were genotyped using the PCR method as described previously.[8,42] All animal care and procedures were performed in accordance with the guidelines of the Institutional Animal Care and Use Committee of Daping Hospital (Chongqing, China).

Cell Culture and siRNA Transfection

Primary calvarial cells were obtained from 4-day-old mice as described previously. Cells were cultured in α-minimum Eagle's medium (MEM) supplemented with 10% fetal bovine serum (FBS), 100 U/mL penicillin, and 100 U/mL streptomycin. The culture medium was changed every 2 days. A series of siRNA (Figure 1A) and a scrambled control siRNA (NC, 5′-TTCTCCGAACGTGTCACG TAA-3′) were synthesized (Ribobio, China). Primary calvarial cells were transiently transfected with 100 mM siRNA using the Lipofectamine 2000 (Invitrogen), according to the manufacturer's instructions. Cell proliferation was detected using an *in vitro* colorimetric assay (Sigma-Aldrich). For the differentiation assay, osteoblasts were plated at 1.0×10^5 cells/well in a 12-well plate, with the medium supplemented with 50 μg/mL L-ascorbic acid and 4 mM Glycerol-2-phosphate. Primary calvarial cells were transfected with 100 mM siRNA and cultured for 2 weeks. Alizarin red and ALP staining was detected using a kit according to the manufacturer's instructions (Sigma-Aldrich). mRNA and protein levels were determined by real-time PCR and western blotting after 48 hr of siRNA transfection.

Culture of Calvarias

Calvarias were cultured according to the literature.[43] Briefly, calvarias were dissected from 5-day-old mice, then they were cut along the midline into two parts. The explants were subsequently cultured in BGJb medium (Gibco) containing 1 mg/mL BSA, 2 mM glutamine, and antibiotics supported by metal grids in a 6-well plate at 37°C in a humidified atmosphere of 5% CO_2 in air. The left parts of calvarias were treated with S2, and right parts were treated with a scrambled control siRNA. After 7 days of culture, the cultured calvarias were fixed with 4% paraformaldehyde (PFA) at 4°C, and then micro-CT scanning was taken for three-dimensional reconstruction. After being decalcified, dehydrated, and embedded in paraffin, coronal sutures were sectioned along the midline of the calvarias at 6-μm intervals and stained with H&E.

Preparation of AAV and Calvarial Injections

AAV2-GFP, AAV5-GFP, AAV9-GFP, and AAV-DJ-GFP were supplied by Hanbio (China). The S2 sequence was subjected to generate AAV9-*Fgfr2*-shRNA (top strand, 5′-AATTCGTCACGACACC GTCCCATCCTTCAAGAGAGGATGGGACGGTGTCGTGATTTT TT-3′; bottom strand, 5′-GATCAAAAAATCACGACACCGTCC CATCCTCTCTTGAAGGATGGGACGGTGTCGTGACG-3′), and

Table 2. Linear Distance Ratios of EDMA for the Comparison between Apert and WT Calvarias Treated with NC or shRNA

Landmarks	NC Apert to WT	shRNA Apert to WT	WT shRNA to NC	Apert shRNA to NC
1 and 2	0.665	0.684	0.978	1.006
1 and 3	0.682	0.703	0.988	1.019
2 and 3	0.761	0.800	0.975	1.024
1 and 4	0.752	0.766	0.989	1.008
2 and 4	1.034	1.021	1.014	1.001
3 and 4	0.842	0.872	0.977	1.012
1 and 5	0.752	0.773	0.992	1.009
2 and 5	0.981	0.983	1.001	1.002
3 and 5	0.951	0.956	0.993	1.006
4 and 5	0.737	0.795	0.953	1.010
1 and 6	0.732	0.740	1.017	1.005
2 and 6	0.935	0.920	1.028	0.996
3 and 6	0.972	0.959	1.024	0.999
4 and 6	0.738	0.777	0.989	1.002
5 and 6	0.780	0.815	1.029	0.991
1 and 7	0.759	0.772	0.984	1.000
2 and 7	0.976	0.994	0.976	0.994
3 and 7	0.833	0.846	0.999	1.014
4 and 7	0.998	1.010	0.988	0.999
5 and 7	0.901	0.920	0.985	1.001
6 and 7	0.863	0.860	1.019	0.999
1 and 8	0.724	0.740	0.984	1.005
2 and 8	0.906	0.932	0.969	0.997
3 and 8	0.917	0.911	1.019	1.012
4 and 8	0.874	0.904	0.971	1.004
5 and 8	0.895	0.915	0.982	1.004
6 and 8	0.887	0.875	1.024	1.003
7 and 8	0.684	0.711	0.965	1.003
1 and 9	0.700	0.744	0.977	1.005
2 and 9	0.877	0.942	0.950	0.995
3 and 9	0.976	0.977	0.995	1.004
4 and 9	0.847	0.906	0.959	1.001
5 and 9	0.908	0.940	0.973	1.000
6 and 9	0.923	0.910	1.014	0.999
7 and 9	0.674	0.745	0.958	1.004
8 and 9	0.623	0.764	0.977	1.014

a scrambled control siRNA (5′-TTCTCCGAACGTGTCACGTAA-3′) was prepared to make AAV-negative control shRNA (NC shRNA top strand, 5′-AATTCGTTCTCCGAACGTGTCACGTAATTCAAGAGATTACGTGACACGTTCGGAGAATTTTTTT-3′; bottom strand, 5′-GATCAAAAAATTCTCCGAACGTGTCACGTAATCTCTTGAATTACGTGACACGTTCGGAGAACG-3′). The expression of either *Fgfr2* shRNA or NC shRNA was driven by U6 promoter, whereas EGFP expression was driven by the cytomegalovirus (CMV) promoter in the AAV9 vector. AAV9-*Fgfr2*-shRNA and AAV9-NC-shRNA viruses were produced. For screening AAV serotypes, the AAV2-GFP, AAV5-GFP, AAV9-GFP, AAV-DJ-GFP, and PBS viruses were injected into the calvarias of post-natal day 0 mice, respectively. AAV9-*Fgfr2*-shRNA and AAV9-N.C-shRNA viruses (Hanbio, China) were locally injected into mouse calvarias twice at day 0 and day 4. 5 μL virus at a concentration of 1.0×10^{12} viral genomes (vg)/mL was used per injection.

Micro-CT Scanning and Analysis

The cultured calvarias and skull samples were scanned with micro-CT (VivaCT40, Scanco Medical, Switzerland), with the condition of 45 kV and 177 μA. Two-dimensional images were used to generate three-dimensional reconstructions. At the same time point, every measurement used the same filtering and segmentation values to obtain three-dimensional images. Identical areas of bone on parietal bones were selected as regions of interest (ROIs) for evaluation by micro-CT Evolution Program version (v.)5.0 software. The parameters included BV, tissue volume (TV), and BMD. Patency of coronal sutures was scored on three-dimensional (3D) skull reconstructions of mice according to the report by Heuzé et al.[44] Four grades of patency were defined: (1) patent, (2) bridging, (3) partially fused, and (4) fused.

Real-Time PCR

Total RNA was extracted from cultured cells or calvarial bone using Trizol reagent (Invitrogen, 15596-026). Single-strand cDNA was synthesized from 1 μg total RNA using the reverse transcriptase kit (Takara). Real-time PCR was performed using the Mx3000 PCR machine (Stratagene, USA) and SYBR Premix ExTaq kit (Takara, RR820A) as standard procedure. The sequences for the primers were as follows: *Fgfr2* forward, 5′-TGCCCTACCTCAAGGTTCTG-3′, *Fgfr2* reverse, 5′-TAGAATTACCCGCCAAGCAC-3′; *Fgfr2-P253R* forward, 5′-TTTCTCCATCAGAACGTTCCCG-3′, *Fgfr2-P253R* reverse, 5′-CGCTGTAAACCTTGCAGACAAAC-3′; *Cbfa1* forward, 5′-GCCACACTTTCCACACTCTC-3′, *Cbfa1* reverse, 5′-CACTTCTGCTTCTTCGTTCTC-3′; *Collagen 1* forward, 5′-CCCGGTGAAAGTGACTGATTC-3′, *Collagen 1* reverse, 5′-ATGGCTTTCATTGGAATTGC-3′; *Osteopontin* forward, 5′-ACACTTTCACTCCAATCGTCC-3′; *Osteopontin* reverse, 5′-TGCCCTTTCCGTTGTTGTCC-3′; *Osteocalcin* forward, 5′-AAGCAGGAGGGCAATAAGGT-3′, and *Osteocalcin* reverse, 5′-TTTGTAGGCGGTCTTCAAGC-3′. All samples were measured in triplicate and normalized to internal control *Cyclophilin* A (forward, 5′-CCACCGACAAGGAGCTAGAGG-3′; reverse, 5′-CCACGCAGAGTGATGGGAAA-3′). The annealing temperature was 56°C.

Western Blotting

Briefly, protein was isolated from the cultured cells using radioimmunoprecipitation assay (RIPA) lysis buffer and then quantitated using a BCA protein quantitative kit (Thermo Fisher Scientific). Equal amounts of protein samples (25 μg) were resolved by 12% SDS-PAGE gel and transferred onto a polyvinylidene difluoride membrane

(Millipore). After being blocked with milk in Tris-buffered saline-Tween buffer, the membrane was probed with primary antibody specific for FGFR2 (Santa Cruz Biotechnology), phospho-ERK1/2 (Cell Signaling Technology), or phospho-P38 (Cell Signaling Technology), followed by secondary antibodies. The signal was detected using chemiluminescence (Thermo Fisher Scientific). The antibody specific for β-actin (Sigma-Aldrich) was applied to normalize the protein loaded. Densitometric analysis of the bands was performed using the ImageJ software.

EDMA

EDMA is a method for quantitatively analyzing the geometric morphology.[45,46] According to Richtsmeier's method,[47] three-dimensional coordinate locations of 9 biologically relevant landmarks located on the calvarias were recorded from three-dimensional CT images of skulls. The collected coordinate data were subjected to WinEDMA software to calculate the FDM (form differences matrix) between Apert and WT mice with NC or shRNA treatment.

Statistical Analysis

The data are presented as means ± SD. Statistical significance was ascertained by two-way ANOVA. When significant levels ($p < 0.05$) were achieved, Tukey's post hoc test was performed (SPSS program version 13.0). The results were considered significant differences at $^{*}p < 0.05$, $^{**}p < 0.01$, $^{\#}p < 0.05$, $^{\#\#}p < 0.01$, $^{※}p < 0.05$, and $^{※※}p < 0.01$.

AUTHOR CONTRIBUTIONS

Study Design, F. Luo, Y.X., X.D., and L.C.; Study Conduct, Z.W., J.H., Q.T., X.S., C.L., N.S., D.Z., M.X., Z.N., W.J., J.C., H.C., S.C., and F. Li; Data Collection, M.L. and M.X.; Data Analysis and Interpretation, F. Luo, Y.X., X.X., C.D., and X.D.; Drafting Manuscript: F. Luo, Y.X., Z.W., and L.C.

CONFLICTS OF INTEREST

The authors have no conflicts of interest.

ACKNOWLEDGMENTS

This work is supported by the National Natural Science Foundation of China (81501848 and 81672125), the Funds for International Cooperation and Exchange of the National Natural Science Foundation of China (81220108020), and the Special Funds for Major State Basic Research Program of China (973 Program, 2014CB942904).

REFERENCES

1. Twigg, S.R., and Wilkie, A.O. (2015). A Genetic-Pathophysiological Framework for Craniosynostosis. Am. J. Hum. Genet. *97*, 359–377.
2. Azoury, S.C., Reddy, S., Shukla, V., and Deng, C.X. (2017). Fibroblast growth factor receptor 2 (FGFR2) mutation related syndromic craniosynostosis. Int. J. Biol. Sci. *13*, 1479–1488.
3. Hehr, U., and Muenke, M. (1999). Craniosynostosis syndromes: from genes to premature fusion of skull bones. Mol. Genet. Metab. *68*, 139–151.
4. Wilkie, A.O., Slaney, S.F., Oldridge, M., Poole, M.D., Ashworth, G.J., Hockley, A.D., Hayward, R.D., David, D.J., Pulleyn, L.J., Rutland, P., et al. (1995). Apert syndrome results from localized mutations of FGFR2 and is allelic with Crouzon syndrome. Nat. Genet. *9*, 165–172.
5. Oldridge, M., Lunt, P.W., Zackai, E.H., McDonald-McGinn, D.M., Muenke, M., Moloney, D.M., Twigg, S.R., Heath, J.K., Howard, T.D., Hoganson, G., et al. (1997). Genotype-phenotype correlation for nucleotide substitutions in the IgII-IgIII linker of FGFR2. Hum. Mol. Genet. *6*, 137–143.
6. Chen, L., Li, D., Li, C., Engel, A., and Deng, C.X. (2003). A Ser252Trp [corrected] substitution in mouse fibroblast growth factor receptor 2 (Fgfr2) results in craniosynostosis. Bone *33*, 169–178.
7. Wang, Y., Xiao, R., Yang, F., Karim, B.O., Iacovelli, A.J., Cai, J., Lerner, C.P., Richtsmeier, J.T., Leszl, J.M., Hill, C.A., et al. (2005). Abnormalities in cartilage and bone development in the Apert syndrome FGFR2(+/S252W) mouse. Development *132*, 3537–3548.
8. Yin, L., Du, X., Li, C., Xu, X., Chen, Z., Su, N., Zhao, L., Qi, H., Li, F., Xue, J., et al. (2008). A Pro253Arg mutation in fibroblast growth factor receptor 2 (Fgfr2) causes skeleton malformation mimicking human Apert syndrome by affecting both chondrogenesis and osteogenesis. Bone *42*, 631–643.
9. Wang, Y., Sun, M., Uhlhorn, V.L., Zhou, X., Peter, I., Martinez-Abadias, N., Hill, C.A., Percival, C.J., Richtsmeier, J.T., Huso, D.L., and Jabs, E.W. (2010). Activation of p38 MAPK pathway in the skull abnormalities of Apert syndrome Fgfr2(+P253R) mice. BMC Dev. Biol. *10*, 22.
10. Holmes, G., Rothschild, G., Roy, U.B., Deng, C.X., Mansukhani, A., and Basilico, C. (2009). Early onset of craniosynostosis in an Apert mouse model reveals critical features of this pathology. Dev. Biol. *328*, 273–284.
11. Du, X., Weng, T., Sun, Q., Su, N., Chen, Z., Qi, H., Jin, M., Yin, L., He, Q., and Chen, L. (2010). Dynamic morphological changes in the skulls of mice mimicking human Apert syndrome resulting from gain-of-function mutation of FGFR2 (P253R). J. Anat. *217*, 97–105.
12. Luo, F., Xie, Y., Xu, W., Huang, J., Zhou, S., Wang, Z., Luo, X., Liu, M., Chen, L., and Du, X. (2017). Deformed Skull Morphology Is Caused by the Combined Effects of the Maldevelopment of Calvarias, Cranial Base and Brain in FGFR2-P253R Mice Mimicking Human Apert Syndrome. Int. J. Biol. Sci. *13*, 32–45.
13. Aldridge, K., Hill, C.A., Austin, J.R., Percival, C., Martinez-Abadias, N., Neuberger, T., Wang, Y., Jabs, E.W., and Richtsmeier, J.T. (2010). Brain phenotypes in two FGFR2 mouse models for Apert syndrome. Dev. Dyn. *239*, 987–997.
14. Martínez-Abadías, N., Percival, C., Aldridge, K., Hill, C.A., Ryan, T., Sirivunnabood, S., Wang, Y., Jabs, E.W., and Richtsmeier, J.T. (2010). Beyond the closed suture in apert syndrome mouse models: evidence of primary effects of FGFR2 signaling on facial shape at birth. Dev. Dyn. *239*, 3058–3071.
15. Nagata, M., Nuckolls, G.H., Wang, X., Shum, L., Seki, Y., Kawase, T., Takahashi, K., Nonaka, K., Takahashi, I., Noman, A.A., et al. (2011). The primary site of the acrocephalic feature in Apert Syndrome is a dwarf cranial base with accelerated chondrocytic differentiation due to aberrant activation of the FGFR2 signaling. Bone *48*, 847–856.
16. Shukla, V., Coumoul, X., Wang, R.H., Kim, H.S., and Deng, C.X. (2007). RNA interference and inhibition of MEK-ERK signaling prevent abnormal skeletal phenotypes in a mouse model of craniosynostosis. Nat. Genet. *39*, 1145–1150.
17. Breik, O., Mahindu, A., Moore, M.H., Molloy, C.J., Santoreneos, S., and David, D.J. (2016). Apert syndrome: Surgical outcomes and perspectives. J. Craniomaxillofac. Surg. *44*, 1238–1245.
18. Kosty, J., and Vogel, T.W. (2015). Insights into the development of molecular therapies for craniosynostosis. Neurosurg. Focus *38*, E2.
19. Morita, J., Nakamura, M., Kobayashi, Y., Deng, C.X., Funato, N., and Moriyama, K. (2014). Soluble form of FGFR2 with S252W partially prevents craniosynostosis of the apert mouse model. Dev. Dyn. *243*, 560–567.
20. Yokota, M., Kobayashi, Y., Morita, J., Suzuki, H., Hashimoto, Y., Sasaki, Y., Akiyoshi, K., and Moriyama, K. (2014). Therapeutic effect of nanogel-based delivery of soluble FGFR2 with S252W mutation on craniosynostosis. PLoS ONE *9*, e101693.
21. Liang, C., Guo, B., Wu, H., Shao, N., Li, D., Liu, J., Dang, L., Wang, C., Li, H., Li, S., et al. (2015). Aptamer-functionalized lipid nanoparticles targeting osteoblasts as a novel RNA interference-based bone anabolic strategy. Nat. Med. *21*, 288–294.
22. Jiang, J., Wakimoto, H., Seidman, J.G., and Seidman, C.E. (2013). Allele-specific silencing of mutant Myh6 transcripts in mice suppresses hypertrophic cardiomyopathy. Science *342*, 111–114.

23. Bongianino, R., Denegri, M., Mazzanti, A., Lodola, F., Vollero, A., Boncompagni, S., Fasciano, S., Rizzo, G., Mangione, D., Barbaro, S., et al. (2017). Allele-Specific Silencing of Mutant mRNA Rescues Ultrastructural and Arrhythmic Phenotype in Mice Carriers of the R4496C Mutation in the Ryanodine Receptor Gene (*RYR2*). Circ. Res. *121*, 525–536.

24. Perrimon, N., Ni, J.Q., and Perkins, L. (2010). In vivo RNAi: today and tomorrow. Cold Spring Harb. Perspect. Biol. *2*, a003640.

25. Deng, Y., Wang, C.C., Choy, K.W., Du, Q., Chen, J., Wang, Q., Li, L., Chung, T.K., and Tang, T. (2014). Therapeutic potentials of gene silencing by RNA interference: principles, challenges, and new strategies. Gene *538*, 217–227.

26. Nguyen, T., Menocal, E.M., Harborth, J., and Fruehauf, J.H. (2008). RNAi therapeutics: an update on delivery. Curr. Opin. Mol. Ther. *10*, 158–167.

27. Zincarelli, C., Soltys, S., Rengo, G., and Rabinowitz, J.E. (2008). Analysis of AAV serotypes 1-9 mediated gene expression and tropism in mice after systemic injection. Mol. Ther. *16*, 1073–1080.

28. Kotterman, M.A., and Schaffer, D.V. (2014). Engineering adeno-associated viruses for clinical gene therapy. Nat. Rev. Genet. *15*, 445–451.

29. Valdmanis, P.N., and Kay, M.A. (2017). Future of rAAV Gene Therapy: Platform for RNAi, Gene Editing, and Beyond. Hum. Gene Ther. *28*, 361–372.

30. Luk, K.D., Chen, Y., Cheung, K.M., Kung, H.F., Lu, W.W., and Leong, J.C. (2003). Adeno-associated virus-mediated bone morphogenetic protein-4 gene therapy for in vivo bone formation. Biochem. Biophys. Res. Commun. *308*, 636–645.

31. Gafni, Y., Pelled, G., Zilberman, Y., Turgeman, G., Apparailly, F., Yotvat, H., Galun, E., Gazit, Z., Jorgensen, C., and Gazit, D. (2004). Gene therapy platform for bone regeneration using an exogenously regulated, AAV-2-based gene expression system. Mol. Ther. *9*, 587–595.

32. Johnson, D., and Wilkie, A.O. (2011). Craniosynostosis. Eur. J. Hum. Genet. *19*, 369–376.

33. Senarath-Yapa, K., Chung, M.T., McArdle, A., Wong, V.W., Quarto, N., Longaker, M.T., and Wan, D.C. (2012). Craniosynostosis: molecular pathways and future pharmacologic therapy. Organogenesis *8*, 103–113.

34. Lei, H., and Deng, C.X. (2017). Fibroblast Growth Factor Receptor 2 Signaling in Breast Cancer. Int. J. Biol. Sci. *13*, 1163–1171.

35. Larson, M.H., Gilbert, L.A., Wang, X., Lim, W.A., Weissman, J.S., and Qi, L.S. (2013). CRISPR interference (CRISPRi) for sequence-specific control of gene expression. Nat. Protoc. *8*, 2180–2196.

36. Rizk, M., and Tüzmen, Ş. (2017). Update on the clinical utility of an RNA interference-based treatment: focus on Patisiran. Pharm. Genomics Pers. Med. *10*, 267–278.

37. Schwarz, D.S., Ding, H., Kennington, L., Moore, J.T., Schelter, J., Burchard, J., Linsley, P.S., Aronin, N., Xu, Z., and Zamore, P.D. (2006). Designing siRNA that distinguish between genes that differ by a single nucleotide. PLoS Genet. *2*, e140.

38. Haley, B., and Zamore, P.D. (2004). Kinetic analysis of the RNAi enzyme complex. Nat. Struct. Mol. Biol. *11*, 599–606.

39. Nasu, T., Ito, H., Tsutsumi, R., Kitaori, T., Takemoto, M., Schwarz, E.M., and Nakamura, T. (2009). Biological activation of bone-related biomaterials by recombinant adeno-associated virus vector. J. Orthop. Res. *27*, 1162–1168.

40. Chen, Y., Luk, K.D.K., Cheung, K.M.C., Xu, R., Lin, M.C., Lu, W.W., Leong, J.C., and Kung, H.F. (2003). Gene therapy for new bone formation using adeno-associated viral bone morphogenetic protein-2 vectors. Gene Ther. *10*, 1345–1353.

41. Chen, Y., Luk, K.D., Cheung, K.M., Lu, W.W., An, X.M., Ng, S.S., Lin, M.C., and Kung, H.F. (2004). Combination of adeno-associated virus and adenovirus vectors expressing bone morphogenetic protein-2 produces enhanced osteogenic activity in immunocompetent rats. Biochem. Biophys. Res. Commun. *317*, 675–681.

42. Schwenk, F., Baron, U., and Rajewsky, K. (1995). A cre-transgenic mouse strain for the ubiquitous deletion of loxP-flanked gene segments including deletion in germ cells. Nucleic Acids Res. *23*, 5080–5081.

43. Garrett, I.R. (2003). Assessing bone formation using mouse calvarial organ cultures. Methods Mol. Med. *80*, 183–198.

44. Heuzé, Y., Singh, N., Basilico, C., Jabs, E.W., Holmes, G., and Richtsmeier, J.T. (2014). Morphological comparison of the craniofacial phenotypes of mouse models expressing the Apert FGFR2 S252W mutation in neural crest- or mesoderm-derived tissues. Bone *63*, 101–109.

45. Richtsmeier, J.T., and Lele, S. (1990). Analysis of craniofacial growth in Crouzon syndrome using landmark data. J. Craniofac. Genet. Dev. Biol. *10*, 39–62.

46. Lele, S., and Richtsmeier, J.T. (1995). Euclidean distance matrix analysis: confidence intervals for form and growth differences. Am. J. Phys. Anthropol. *98*, 73–86.

47. Richtsmeier, J.T., Baxter, L.L., and Reeves, R.H. (2000). Parallels of craniofacial maldevelopment in Down syndrome and Ts65Dn mice. Dev. Dyn. *217*, 137–145.